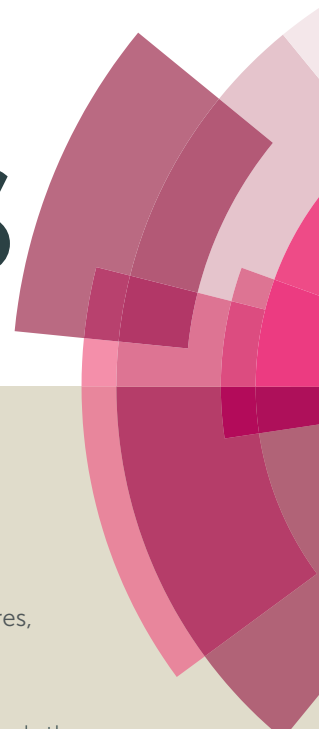


RSC Advances



This article can be cited before page numbers have been issued, to do this please use: P. Prieto, I. Torres, J. R. Carrillo, A. Diaz, R. Martín, M. V. Gómez, L. Stegemann, C. Strassert, J. Orduna, J. Buendía, E. E. Greciano, J. S. Valera, E. Matesanz and L. Sanchez, *RSC Adv.*, 2016, DOI: 10.1039/C6RA02473D.



This is an *Accepted Manuscript*, which has been through the Royal Society of Chemistry peer review process and has been accepted for publication.

Accepted Manuscripts are published online shortly after acceptance, before technical editing, formatting and proof reading. Using this free service, authors can make their results available to the community, in citable form, before we publish the edited article. This *Accepted Manuscript* will be replaced by the edited, formatted and paginated article as soon as this is available.

You can find more information about *Accepted Manuscripts* in the [Information for Authors](#).

Please note that technical editing may introduce minor changes to the text and/or graphics, which may alter content. The journal's standard [Terms & Conditions](#) and the [Ethical guidelines](#) still apply. In no event shall the Royal Society of Chemistry be held responsible for any errors or omissions in this *Accepted Manuscript* or any consequences arising from the use of any information it contains.



Journal Name

ARTICLE

Self-assembly of T-shape 2H-benzo[d][1,2,3]-triazoles. Optical waveguide and photophysical properties†

I. Torres,^a J. R. Carrillo,^a A. Díaz-Ortiz,^a R. Martín,^a M. V. Gómez,^a L. Stegemann,^b C. A. Strassert,^b J. Orduna,^c J. Buendía,^d E. E. Greciano,^d J. S. Valera,^d E. Matesanz,^e L. Sánchez*^d and P. Prieto*^a

Received 00th January 20xx,
Accepted 00th January 20xx

DOI: 10.1039/x0xx00000x

www.rsc.org/

T-shaped 2H-benzo[d][1,2,3]triazole derivatives have been synthesized by Sonogashira coupling reactions under microwave irradiation. DFT calculations were performed in order to understand the structure-property relationships – an aspect that is of vital importance for the rational design of organic self-assemblies for optoelectronic applications. Concentration-dependent ¹H Pulse Field-Gradient Spin-Echo (PFGSE) NMR spectroscopy and UV/Vis spectrophotometry indicated the absence of a tendency for the aggregation of single molecules in solution. In contrast, in the solid state these compounds form organized aggregates and these were studied by scanning electron microscopy (SEM), which showed the influence that the peripheral substitution has on the morphology of the aggregates. For example, methoxy-substituted benzotriazoles self-assemble into thick and crystalline needle-like structures. However, the unsubstituted triazoles give rise to flower-like aggregates. Interestingly, the aggregates formed by benzotriazole **1c** exhibit waveguide properties.

Introduction

Organic electronics is a research area that has had a significant impact in the last two decades owing to the development of semiconducting materials and innovation in technological devices. This is expected to be a powerful and fascinating technology that offers great differentiation from the conventional electronic applications based on inorganic materials.¹ In this framework, organic materials that exhibit strong emission in the solid state have received increasing attention in recent years because of their potential applications in optical and optoelectronic devices such as optical waveguides,² optically pumped lasers³ and light-emitting diodes.⁴ The transmission of light in fibers is an exciting challenge in the information age and, as a consequence, investigations in this field have become very attractive.⁵

Optical waveguides are structures that have a higher refractive index than the environment. As a consequence, these materials can retain light as they transmit it internally by total reflection at the interface. These materials are capable of propagating and manipulating light efficiently on the subwavelength scale. These 1D-nanostructures can be built by self-assembly of organic molecules through non-covalent bonds such as hydrogen bonds, van der Waals interactions, π - π stacking or CH- π interactions, and they are highly ordered systems.

A common feature of organic waveguides is the presence of heteroaromatic rings with nitrogen atoms, which have a marked influence on the formation of supramolecular structures.⁶ 1,2,4-Triazole systems have proven to have excellent electron-transporting and hole-blocking abilities due to the presence of this highly electron-deficient moiety. Another important feature of this moiety is its ability to form a variety of non-covalent interactions. Accordingly, a large number of 1,2,4-triazole derivatives have been described with a variety of uses in materials science.⁷ Moreover, 1,2,4-triazole rings tend to decrease the effective π -conjugation of aromatic systems, thus facilitating the design of blue emitters.⁸ Recently, our research group has reported the synthesis of 4-aryl-3,5-bis(arylethynyl)-4H-1,2,4-triazole⁹ and 4-aryl-3,5-bis(arylethynyl)aryl-4H-1,2,4-triazole derivatives¹⁰ and their aggregation, in which C-H... π interactions play a role.

In order to obtain such promising materials it is very important to apply a rational design process. In this sense, computational

^a Departamento de Q. Inorgánica, Q. Orgánica y Bioquímica. Facultad de Ciencias y Tecnologías Químicas. Universidad de Castilla-La Mancha. 13071- Ciudad Real. Spain. E-mail: mariapilar.prieto@uclm.es. Fax: +34 926295318.

^b Physikalisches Institut and Center for Nanotechnology (CeNTech). Universität Münster. Heisenbergstrasse 11, 48149 Münster. Germany.

^c Departamento de Química Orgánica. Facultad de Ciencias-Instituto de Ciencias de Materiales de Aragón. Universidad de Zaragoza-CSIC. 50009-Zaragoza. Spain.

^d Departamento de Química Orgánica. Facultad de Ciencias Químicas. Universidad Complutense de Madrid. 28040-Madrid. Spain. E-mail: lusamar@quim.ucm.es.

^e C.A.I. Difracción de Rayos X. Facultad de Ciencias Químicas. Universidad Complutense de Madrid. 28040-Madrid. Spain.

† Electronic Supplementary Information (ESI) available. See DOI: 10.1039/x0xx00000x

ARTICLE

Journal Name

chemistry¹¹ is a powerful tool that allows us to determine properties of the building blocks and aggregates to avoid unnecessary synthesis, thereby minimizing the cost and environmental impact. In this sense, the use of sustainable methods is a factor that needs to be considered.

As part of our ongoing research program, and in an effort to increase our knowledge of optical waveguides, we carried out the design, computational study and synthesis of 2*H*-benzo[d][1,2,3]triazole derivatives. Due to the excellent properties shown by the 4*H*-1,2,4-triazole derivatives, we decided to study the benzotriazole moiety with the aim of retaining the ability of these systems to self-assemble while varying their emission: the benzotriazole system does not break the effective π -conjugation of aromatic systems and it could provide compounds with different photophysical properties. Furthermore, our previously described compounds^{9,10} are V-shaped whereas benzotriazoles adopt a T-shape. It is known that optoelectronic properties are highly dependent on the chemical structure and on the supramolecular aggregation. Theoretical models can be used to predict optical properties and are useful for the efficient *in silico* design of new compounds.

Results and discussion,

The work described here was focused on the synthesis and applications of different 2*H*-benzo[d][1,2,3]triazole derivatives (Fig. 1).

Computational study

Prior to carrying out the chemical synthesis, our initial goal was to determine the properties and propensity for self-assembly of

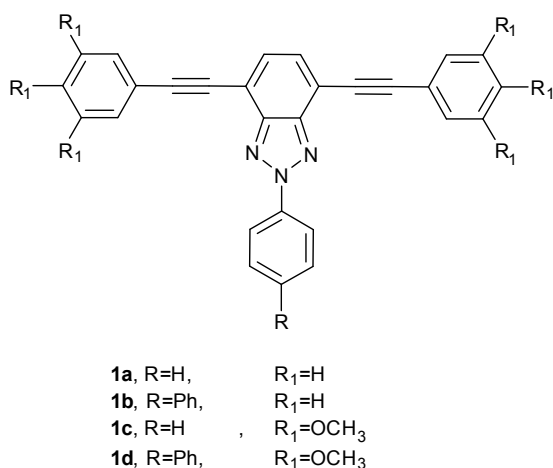


Fig. 1 2*H*-Benzo[d][1,2,3]triazole derivatives

these compounds using computational chemistry. We initially calculated the UV-vis absorption spectra of compounds **1**. The

Table 1. λ_{abs} and λ_{em} and energies of HOMO-LUMO calculated at CPCM-M06-2X/6-311+G(2d,p)

Compound	λ_{abs} (nm)	λ_{em} (nm)	E_{HOMO} (eV)	E_{LUMO} (eV)	Band gap (eV)
1a	392.3	484.6	-7.06	-2.05	5.01
1b	367.5	485.8	-7.06	-2.07	4.99
1c	402.0	498.3	-6.90	-2.04	4.86
1d	397.8	494.2	-6.89	-2.07	4.82

calculated λ_{abs} and λ_{em} values are collected in Table 1 (see spectra in Electronic Supplementary Information, Fig. S1). The electronic spectra were also calculated in dichloromethane solution using the conductor-like polarizable continuum model (CPCM)¹² and the time-dependent density functional theory (TD-DFT) approach.¹³ The M06-2X¹⁴ meta-exchange functional was employed. The choice of this functional was based on the accurate results obtained in the calculation of systems with high spatial orbital overlap, which are even better than those provided by the more widely used CAM-B3LYP.¹⁵ The energies of frontier molecular orbitals are also collected in Table 1.

The topologies of the FMO are very similar in compounds **1a–d**. The HOMO is located in the horizontal branch and the LUMO in both branches, mainly in the vertical one (Fig. 2). Additionally, the introduction of methoxy-substituents only affects the value of the HOMO and this leads to a decrease in the bandgap (Table 1, entry 1 vs 3, and 2 vs 4).

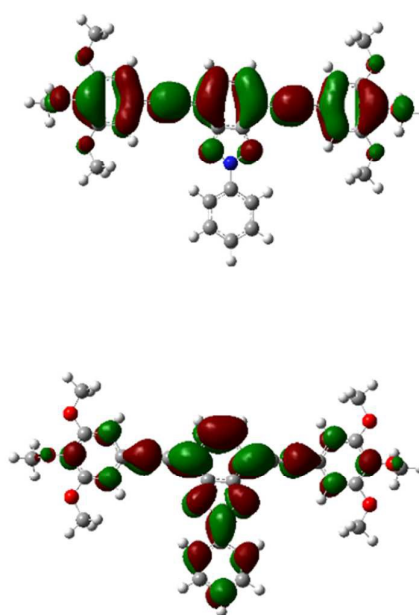


Fig. 2

HOMO-LUMO topologies of compound **1c**.

Secondly, the structure of the molecular stacks was studied by applying Grimme's B97D functional,¹⁶ which includes the

dispersion forces. The 6-31G* basis set was employed.¹⁷ In order to simplify this study, 2-phenyl-2H-benzo[d][1,2,3]triazole (**2a**) and 2-biphenyl-2H-benzo[d][1,2,3]triazole (**2b**) were chosen as model compounds. The π -stacking arrangement considered for the calculations is depicted in Fig. 3. The relevant intermolecular parameters are as follows: (i) the distance R refers to the distance between the centers of mass of the two triazole rings and indicates the separation between the two benzotriazole rings; (ii) θ is the dihedral angle between the two rings and denotes the relative orientation of the rings, *i.e.*, the benzotriazoles are parallel and antiparallel when $\theta = 0^\circ$ and $\theta = 180^\circ$, respectively; (iii) ϕ corresponds to the angle formed by the planes of the two rings and indicates the degree of tilting, *i.e.*, the two rings are coplanar when $\phi = 0^\circ$, while $\phi = 180^\circ$ corresponds to a perpendicular T-shaped configuration; (iv) the parameter Δd defines the displacement of the two benzotriazole moieties in the dimer.

The optimized dimers of 2-phenyl-2H-benzo[d][1,2,3]triazole (**2a**) and 2-biphenyl-2H-benzo[d][1,2,3]triazole (**2b**) are shown in Fig. 4. The presence of the phenyl or biphenyl units results in different aggregation pathways.

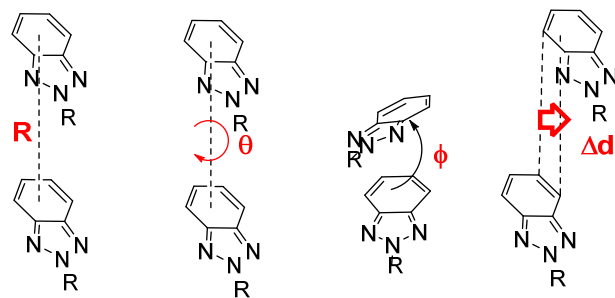


Fig. 3 Structure of the π -stacked benzotriazole dimer and indication of the intermolecular parameters according to Ref.¹⁸

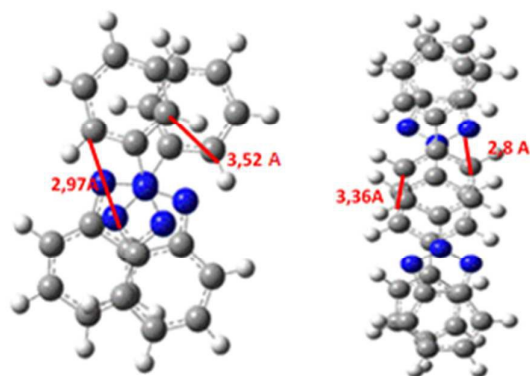


Fig. 4 Different stacking of **2a** (left) and **2b** (right) dimers computed at B97D/6-31+G*.

The benzotriazole units in the dimer of *N*-phenylbenzotriazole **2a** are rotated slightly in order to avoid electrostatic repulsion

between these electron-rich fragments. The aromatic C–H bond in the *ortho* position of the *N*-phenyl unit of one molecule is involved in weak H-bonding (2.97 Å) with the sp^2 nitrogen atom of the adjacent molecule, and a CH- π interaction also occurs with another *N*-phenyl unit (3.52 Å). CH- π interactions can also be observed between the *ortho* protons of one benzotriazole ring and the benzotriazole ring of a neighbouring molecule.

In the dimer of compound **2b**, the π - π stacking between the biphenyl units (3.36 Å) and H-bonding (2.8 Å) of the *ortho*-H of the biphenyl of one molecule with the sp^2 nitrogen atom of the adjacent molecule are the non-covalent forces that direct the self-assembly of this compound. This outcome is consistent with our previous study on the optical waveguide properties of triazole derivatives.^{9,10}

We subsequently introduced the arylacetylenic fragment in the basic models and the two possible aggregates were optimized, head-to-head and vertical ones. The calculated structures (Fig. S2) showed that the triple bonds play an important role in the stabilization of both aggregates, due to the formation of CH- π interaction between the *sp* carbon and the aromatic *ortho*-proton and the benzotriazole protons. Another stabilizing interaction is the CH- π between different aromatic protons and aromatic carbons. It is interesting to note that in these structures there are no hydrogen bonding interactions. Thereby, it can be deduced that the triple bond plays a more important role than the presence of nitrogen atoms in the stabilization of the aggregates. Only the head-to-head aggregate of the biphenyl derivative (**1b**) showed different behaviour. In this case, π - π stacking and H-bonding are the most important interactions. Finally, the next goal was to analyse the role played by the methoxy framework. The optimized horizontal and vertical aggregates for phenyl (**1c**) and biphenyl derivatives (**1d**) are depicted in Fig. 5. It is interesting to note that in this case the H-bonding between the oxygen of one methoxy group and the hydrogen of the methoxy group of the adjacent molecule (2.54 Å) and the CH- π interaction of the *sp* carbon of the triple bond and the CH₃ methoxy group are the most important interactions that govern the formation of aggregates. The dimer of **1c** was used as a model and careful analysis of the optimized structures again led to the conclusion that the head-to-head aggregate is more organized and stable than the vertical one.

It can be concluded that these compounds have several non-covalent interactions that allow them to form good molecular aggregates. So, the identification of optoelectronic and self-assembly properties in these derivatives prompted us to address the chemical synthesis of these compounds.

ARTICLE

Journal Name

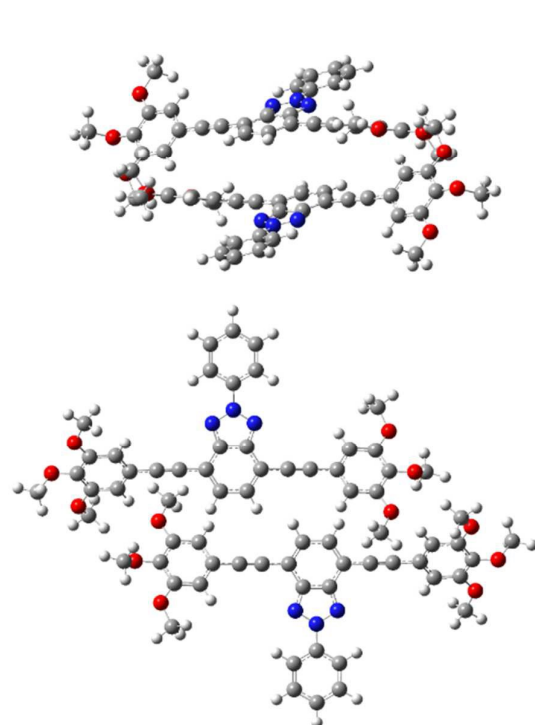
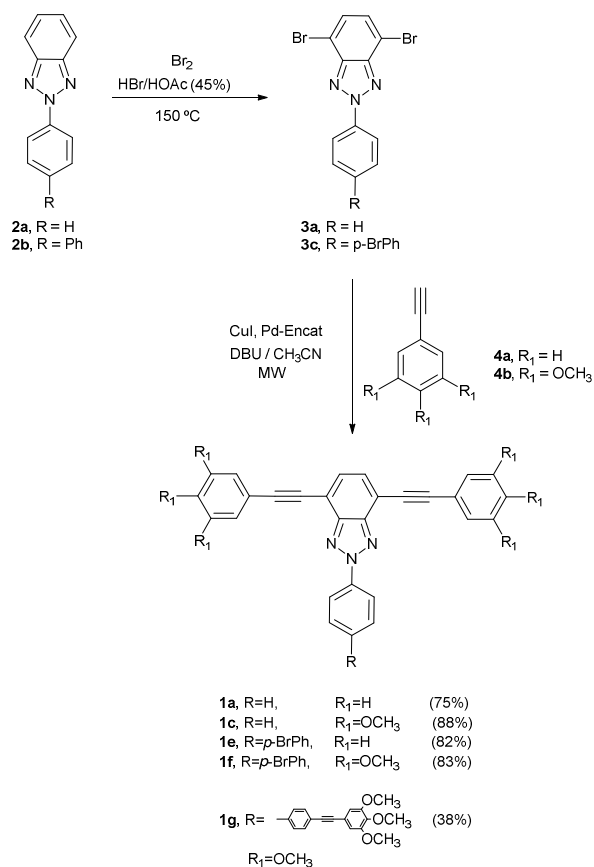


Fig. 5 Optimized structures of the vertical aggregate (top) and head-to-head aggregate (bottom) of compounds **1c** and **1d** computed at B97D/6-31G*

Chemical synthesis

Benzotriazoles **2a,b** were prepared from 1-nitro-2-nitrosobenzene and aniline or (1,1'-biphenyl)-4-amine, respectively, according to the synthetic procedure described by Höger.¹⁹ Bromination of these compounds afforded the bromobenzotriazoles **3a,c** in 80% and 97% yield, respectively. However, while **2a** gave only a dibromo-derivative, **2b** led to a tribromobenzotriazole (**3c**) although the excess of bromine had been significantly reduced. Compound **3b** (4,7-dibromo-2-phenyl-2H-benzo[d][1,2,3]triazole) could not be obtained under any of the reaction conditions employed (Scheme 1).

The Sonogashira C–C cross-coupling reaction between bromobenzotriazoles **3** and arylacetylenes **4** using reusable Pd-EnCat™ TPP30, 1,5-diazabicyclo[5.4.0]undecene-5-ene (DBU), CuI and MW irradiation as the energy source afforded arylalkynylbenzotriazoles **1** within 20 minutes in good yields (up to 88%)¹⁰ (Scheme 1). We recently developed this sustainable procedure for the preparation of arylalkynylaryl-1,2,4-triazoles.⁹ The cross-coupling reaction between **3c** and 5-ethynyl-1,2,3-trimethoxybenzene (**4b**) under more energetic reaction conditions (170 °C) provided the trisubstituted benzotriazole **1g**, albeit in moderate yield. However, a similar reaction with phenylacetylene was unsuccessful, perhaps due to the high degree of polymerization under these reaction conditions. All of the compounds described above gave satisfactory spectroscopic and analytical data.



Scheme 1. Synthesis of 2H-benzo[d][1,2,3]triazole derivatives **1**. Isolated yields in brackets.

Photophysical characterization

A thorough photophysical study was carried out in order to demonstrate experimentally the theoretical predictions. The UV/Vis absorption and emission spectra in solution at room temperature were studied first (Fig. 6).

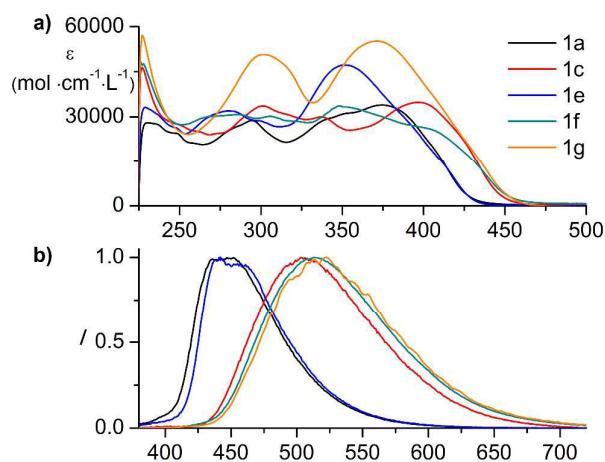


Fig. 6 a) Absorption spectra in DCM. b) Emission spectra at room temperature in DCM.

Table 2. Photophysical data for the benzotriazole derivatives in dichloromethane at room temperature.

	solution			
	λ_{abs} (nm)	λ_{em} (nm)	$\tau^{[\text{a}]}$ (ns)	Φ
1a	374	442	2.586	0.55
1c	397	503	3.434	0.65
1e	352	441	2.665	0.54
1f	349 / 408 (sh)	513	3.735	0.57
1g	372	522	3.785	0.82

^[a] Intensity weighted average lifetime

Excitation and emission spectra of frozen glassy matrices at 77 K and of the amorphous solids, along with the corresponding excited state lifetime decays, are depicted in Fig. S3 in the Supporting Information. The most significant photophysical data are summarized in Table 2. It can be clearly observed that the introduction of MeO-groups on the phenyl substituents leads to destabilization of the HOMO, as also observed from the computational results, and thus to red-shifted absorption and emission spectra for **1c**, **1f** and **1g** as compared to **1a** and **1e**. In contrast, the introduction of the Br-phenyl group does not appreciably affect the photophysical properties. The concomitant broadening of the emission spectra of **1c**, **1f** and **1g** is caused by an enhanced charge-transfer character due to the presence of the MeO-groups, which favours the relocation of the electronic density from the side arms (HOMO) and the dipole-mediated coupling with the surrounding solvent molecules. Interestingly, these electron-donating groups also lead to prolonged excited state lifetimes and higher photoluminescence quantum yields, which indicate that the radiationless deactivation rate is decreased. At 77 K the structured vibrational progression is recovered as the charge-transfer character is less favoured due to the lack of solvent reorientation to stabilize the polar excited state. The agreement between the theoretical and experimental absorption and emission spectra is excellent.

Self-assembly study

Following our initial goal, the aggregation of the reported 2*H*-benzo[d][1,2,3]triazoles was investigated both in solution and solid state. As in our previous reports on 4*H*-1,2,4-triazoles, compounds **1** had a very low tendency to aggregate in solution.^{9,10} In good analogy with those reports, appreciable changes in the ¹H NMR spectra of 2*H*-benzo[d][1,2,3]triazole **1** were not observed on varying the concentration in a good solvent like chloroform.

Concentration-dependent ¹H NMR measurements were carried out on compounds **1a** and **1c** (Fig. S4 and Fig. 7, respectively) in CDCl₃ at 298 K. Variation in chemical shifts cannot be observed in Fig. S4 for the different protons of compound **1a**.

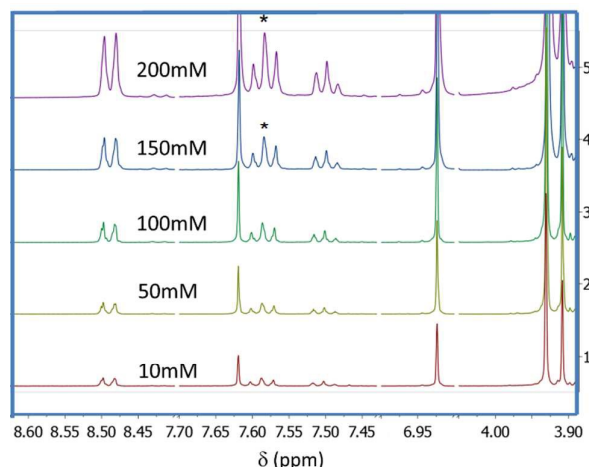


Fig. 7 Collection of ¹H NMR spectra of compound **1c** in CDCl₃ at 298 K. Some regions (8.40–7.70; 7.43–7.00 ppm; 6.90–4.05 ppm; 3.90–0 ppm) have been removed in order to show all of the signals within the Fig. TMS was used as internal standard.

Similarly, clear evidence for a tendency to aggregation of benzotriazole **1c** in a solution of CDCl₃ cannot be seen in Figure 7. Two peaks (marked with an asterisk in Fig. 7) show a negligible chemical shift change of only 0.01 ppm with respect to the spectra of the more dilute samples when the concentration reaches very high values (150–200 mM).

Concentration-dependent ¹H Pulsed Field-Gradient Spin-Echo (PFGSE) NMR spectroscopy experiments²⁰ were performed on compound **1c** in CDCl₃ at 298 K using CH₃ as internal standard. The aim of these experiments was to confirm the absence of any tendency to aggregation of single molecules in solution, as shown by the concentration-dependent ¹H NMR experiments. The translational self-diffusion coefficients (D_t) can be evaluated by PFGSE NMR experiments to provide information concerning the molecular size in solution and therefore about the existence of an aggregation process as the concentration increased.²¹ The diffusion coefficients for each solution of compound **1c** are shown in Table 3. The D_t values ($\text{m}^2 \text{s}^{-1}$) for the different concentrations are not significantly different, thus confirming the lack of aggregation in solution. The changes in solution viscosity within the concentration range studied (75–10 mM) are expected to be negligible²¹ and within the error observed for the diffusion coefficient Dt ($\text{m}^2 \text{s}^{-1}$).

Table 3. Diffusion coefficients ($10^{-10} D_t$, $\text{m}^2 \text{s}^{-1}$) and concentrations (C , mM) for compound **1c** in CDCl₃ at 298 K

C [mM]	D_t [$\text{m}^2 \text{s}^{-1}$]
10	5.0 ± 0.36
25	5.6 ± 0.43
50	5.5 ± 0.46
75	5.1 ± 0.5

Fig. 9 (a) X-ray crystal structure of compound **1c**. (b-d) C–H... π intermolecular interactions operating in the aggregation of compound **1c**

(Fig. 9b). The unit cell consists of two of these trimers interacting, once again, through C–H... π interactions between the methoxy groups and one of the *sp* carbons of the ethynyl linker, with the benzotriazole units rotated by 180° (Fig. 9c). Unfortunately, the thick aggregates obtained from benzotriazole **1f** were not suitable for X-ray analysis.

The calculated dimer and the structure obtained by X-ray analysis are consistent with one another (Fig. 5b and 9c). It can therefore be concluded that the computational calculations, although unable to determine the exact structure of the aggregates, represent an excellent tool to predict the interactions that govern the formation of aggregates and for the design of cores with possible auto-aggregation behavior.

Considering the previously reported data on the optical waveguiding features of related triazoles,^{9,10} we investigated the propagation of light in the aggregates formed by benzotriazoles **1c** and **1f**. These studies were carried out using a confocal optical microscope and the aggregates of **1c** and **1f** were irradiated with a laser beam. The resulting fluorescence images were collected with a camera. Interestingly, only the aggregates formed by benzotriazole **1c** showed propagation of the incident light along the rod-like aggregate. Thus, propagated light was observed at the extremes of the aggregates of **1c** when the light was directed on the middle of such aggregates (Fig. 10). However, the supramolecular structure formed by **1f** did not exhibit any optical waveguiding behavior and irradiation with a laser beam of the aggregates formed by this benzotriazole did not result in the propagation of the incident light (Fig 10b).

Finally, a photophysical study of these aggregates was performed. The UV/Vis absorption and emission spectra of the crystalline aggregates are shown in Fig. 11. The most significant photophysical data are summarized in Table 4. Interestingly, a clear vibrational progression can be observed for **1e** also in amorphous solid, whereas the broad, unstructured emission is recovered in the aggregated form. In general, the

Fig. 10 Polarized light (PL) microscopy images of the aggregates of **1c** (a, b); and **1f** (c, d) obtained by irradiating the entirety (left) or a portion (right) of the aggregate

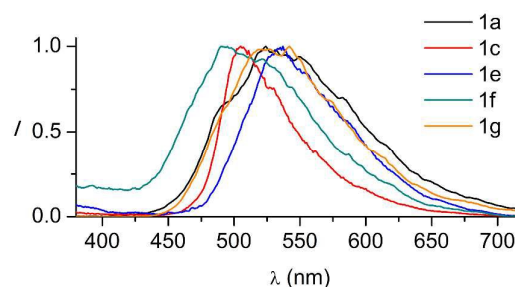


Fig. 11 The UV/Vis absorption and emission spectra of the crystalline aggregates **1a-g**

Table 4. Photophysical data for benzotriazole aggregates

	λ_{abs} (nm)	λ_{em} (nm)	$\tau^{[a]}$ (ns)	Φ
1a	374	524	1.936	0.10
1c	397	505	2.246	0.16
1e	352	537	1.799	0.13
1f	349 / 408 (sh)	490	1.572	0.05
1g	372	542	2.175	0.01

[a] intensity weighted average lifetime.

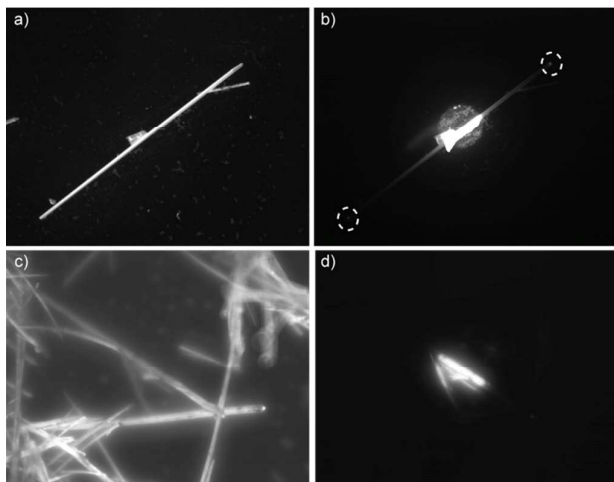
solid state spectra (both amorphous powders and crystalline aggregates) show narrower emission ranges and lower fluorescence quantum yields than the corresponding solutions, probably due to the lower charge-transfer character of the excited state in the absence of stabilizing solvent molecules. Notably, the emission maxima of **1a** and **1c** appear red-shifted into the spectral region of **1e**, **1f** and **1g** with comparable excited state lifetimes. In the case of **1f** the emission peak is blue-shifted when compared to fluid solutions, unchanged for **1c** and slightly red-shifted for **1g**. It is clear that the intermolecular interactions in the solid state affect **1a** and **1e** to a greater extent than for the MeO-substituted species.

Conclusions

In summary, after computational design, 2H-benzo[d][1,2,3]triazoles were synthesized using sustainable methods where possible, i.e., a marked decrease in the amount of solvent employed, a reusable catalyst and microwave irradiation as the energy source.

DFT calculations at the B397D/6-31G* level on these T-shaped heterocyclic derivatives provided a dimer structure that is consistent with that determined by X-ray analysis. The findings indicate that the compounds are able to form supramolecular structures through CH- π interactions and H-bonding arrays.

Regarding the photophysical properties of the compounds, the introduction of MeO groups on the phenyl rings led to destabilization of the HOMO according to the computational results and thus to red-shifted absorption and emission spectra.



ARTICLE

Journal Name

Concentration-dependent ^1H Pulse Field-Gradient Spin-Echo (PFGSE) NMR spectroscopy indicated the absence of any tendency to aggregation for single molecules in solution.

As observed previously, these compounds aggregate in the solid state – as determined by the slow diffusion technique on using CHCl_3 as good solvent and a variety of poor solvents such as acetonitrile, hexane or methanol. The as-prepared organized aggregates were visualized by scanning electron microscopy (SEM) on glass substrates and this demonstrated the influence exerted by the peripheral substitution on the morphology of these aggregates. Methoxy-substituted benzotriazoles **1c** and **1f** self-assemble to form thick and crystalline needle-like structures. However, SEM images show that the unsubstituted triazoles give rise to flower-like aggregates. It is noteworthy that the aggregate of compound **1g** shows similar behavior, probably due to the interdigitation of the methoxy groups.

Interestingly, the aggregates formed by benzotriazole **1c** exhibit waveguide properties that allow the propagation of incident light along the rod-like aggregate. Thus, propagated light is observed at the extremes of the aggregates of **1c** when the light is directed onto the middle of such aggregates

Experimental

General methods. Reagents were used as purchased. All air-sensitive reactions were carried out under an argon atmosphere. Microwave irradiations were performed in a Discover[®] (CEM) focused microwave reactor. Measurements and temperature control were performed with an infrared reader and parameters were recorded using the program designed by CEM. Flash chromatography was performed using silica gel (Merck, Kieselgel 60, 230–240 mesh or Scharlau 60, 230–240 mesh). Analytical thin layer chromatography (TLC) was performed using aluminium-coated Merck Kieselgel 60 F254 plates. NMR spectra were recorded on a Varian Unity 500 (^1H : 500 MHz; ^{13}C : 125 MHz) spectrometer at 298 K using partially deuterated solvents as internal standards. Coupling constants (J) are denoted in Hz and chemical shifts (δ) in ppm. Multiplicities are denoted as follows: s = singlet, d = doublet, t = triplet, m = multiplet, br = broad.

MALDI-TOF mass spectra were measured on a Bruker Autoflex II TOF/TOF spectrometer (Bremen, Germany) using dithranol as the matrix. Samples co-crystallized with the matrix on the probe were ionized with a nitrogen laser pulse (337 nm) and accelerated under 20 kV with time-delayed extraction before entering the time-of-flight mass spectrometer. Matrix (10 mg/mL) and sample (1 mg/mL) were separately dissolved in methanol and mixed in a matrix/sample ratio ranging from 100:1 to 50:1. Typically, a 5 μL mixture of matrix and sample was applied to a MALDI-TOF MS probe and air-dried. MALDI-TOF MS in positive reflector mode was used for all samples. External calibration was performed by using Peptide Calibration Standard II (covered mass range: 700–3200 Da), Protein Calibration Standard I (covered mass range: 5000–17500 Da) and Protein Calibration Standard II (covered mass range: 20000–70000 Da) from Care (Bruker). The applied peak

(m/z determination) detection method was the threshold centroid at 50% height of the peak maximum.

SEM images were obtained on a JEOL JSM 6335F microscope working at 10 kV. The samples for SEM imaging were prepared by a controlled precipitation using the appropriate solvent or by slow diffusion by using mixtures of solvents, depending on their solubility properties (see the corresponding Figure Caption for a detailed description). The corresponding solid was deposited onto a glass substrate and the remaining solvent was evaporated slowly.

PL photomicrographs and optical waveguide photomicrographs were obtained on a Zeiss Axioplan-2 microscope with a CCD camera. A laser with an excitation source of 488 or 532 nm wavelength was employed for the measurements. Illumination of the aggregates of **1** with a laser beam generated a strong emission in the irradiated area. In addition, a brilliant emission point was clearly observed at the extremes/edges of the aggregates due to the propagation of laser light.

Photophysical Data

Absorption spectra were measured on a Varian Cary 5000 double-beam UV-Vis-NIR spectrophotometer and were baseline-corrected. Steady-state excitation and emission spectra were recorded on a FluTime300 spectrometer from PicoQuant equipped with a 300 W ozone-free Xe lamp (250–900 nm), a 10 W Xe flash-lamp (250–900 nm, pulse width < 10 μs) with repetition rates of 0.1–300 Hz, an excitation monochromator (Czerny-Turner 2.7 nm/mm dispersion, 1200 grooves/mm, blazed at 300 nm), diode lasers (pulse width < 80 ps) operated by a computer-controlled laser driver PDL-820 (repetition rate up to 80 MHz, burst mode for slow and weak decays), two emission monochromators (Czerny-Turner, selectable gratings blazed at 500 nm with 2.7 nm/mm dispersion and 1200 grooves/mm, or blazed at 1250 nm with 5.4 nm/mm dispersion and 600 grooves/mm), Glan-Thompson polarizers for excitation (Xe-lamps) and emission, a Peltier-thermostated sample holder from Quantum Northwest (–40 $^\circ\text{C}$ –105 $^\circ\text{C}$), and two detectors, namely a PMA Hybrid 40 (transit time spread FWHM < 120 ps, 300–720 nm) and a R5509-42 NIR-photomultiplier tube (transit time spread FWHM 1.5 ns, 300–1400 nm) with external cooling (–80 $^\circ\text{C}$) from Hamamatsu. Steady-state and fluorescence lifetimes were recorded in TCSPC mode by a PicoHarp 300 (minimum base resolution 4 ps). Emission and excitation spectra were corrected for source intensity (lamp and grating) by standard correction curves. Lifetime analysis was performed using the commercial FluoFit software. The quality of the fit was assessed by minimizing the reduced chi-squared function (χ^2) and visual inspection of the weighted residuals and their autocorrelation. Luminescence quantum yields were measured with a Hamamatsu Photonics absolute PL quantum yield measurement system (C9920-02) equipped with a L9799-01 CW Xenon light source (150 W), monochromator, C7473 photonic multi-channel analyzer, integrating sphere and employing U6039-05 PLQY measurement software

(Hamamatsu Photonics, Ltd., Shizuoka, Japan). All solvents used were of spectrometric grade.

Computational study

All calculations included in this paper were carried out using the GAUSSIAN 09²² series of programs. In order to include electron correlation at a reasonable computational cost, Density Functional Theory (DFT)²³ was used. The structures were fully optimized by means of the B97D¹⁶ method with the standard 6-31G(d) basis set¹⁷ until the minima were achieved. The nature of all the stationary points was checked by computing vibrational frequencies, and all the species were found to be true potential energy minima, as no imaginary frequency was obtained (NImag = 0).

For the electronic study the equilibrium geometries were obtained using the M06-2X¹⁴ hybrid meta-GGA exchange-correlation functional with the 6-31G(d) basis set both for ground and first excited states. Solvent effects were estimated using the Conductor-like Polarizable Continuum Model (CPCM)¹² with dichloromethane as solvent. Excitation energies were calculated by time-dependent single point calculations using the M06-2x/6-311+G(2d,p) model chemistry. Vertical excitation energies were calculated at the optimized ground (Absorption) or Excited (Emission) state geometry. Molecular orbital contour plots were obtained using the Gausview software.

Concentration-dependent ¹H NMR experiments were carried out for compounds **1a** and **1c** at 298 K. Concentration-dependent ¹H PFGSE (Pulsed Field Gradient Spin Echo) measurements were performed on compound **1c** in CDCl₃ at 298 K using the DOSY bipolar pulse pair stimulated echo with convention compensation (Dbppste_cc in the Varian DOSY package) in a concentration range from 10 mM to 75 mM. The Doneshot pulse sequence was used for the gradient calibration by means of the diffusion of HDO in D₂O at 298 K. The correction for gradient non-uniformity was employed to process each spectrum. The signal intensities as a function of a delay parameter (del2) (velocity map) were measured to corroborate the absence of convention using the Dbppste_cc pulse sequence. The same acquisition parameters were used for the whole concentration range: 30 increments in the gradient strength (3000–22000), 64 averages per increment step, duration of the magnetic field pulse gradient (δ) of 2 ms, a diffusion time (Δ) of 40 ms, and a pre-acquisition delay of 3 s. Reference deconvolution (FIDDLE) on CH₃I (internally added) was used to correct the line shapes.

Preparation of 2-aryl-4,7-bis(arylethynyl)-2H-benzo[d][1,2,3]triazoles. **General procedure:** A mixture of 2-aryl-4,7-dibromo-2H-benzo[d][1,2,3]triazole (**3**) (1 eq), the corresponding acetylene derivative (**4**) (2 or 3.5 eq), DBU (2 eq), Cul (0.05 eq) and Pd-EncatTM TPP30 (0.035 eq) was charged under argon to a dried microwave vessel. CH₃CN (1 mL) was added. The vessel was closed and irradiated at 130 °C (170 °C in the case of **1g**) for 20 min. The crude product was purified by column

chromatography, eluting with hexane/ethyl acetate (9:1), to give analytically pure products **1**.

2-Phenyl-4,7-bis(phenylethynyl)-2H-benzo[d][1,2,3]triazole

(1a): From 4,7-dibromo-2-phenyl-2H-benzo[d][1,2,3]triazole (**3a**) (0.100 g, 0.28 mmol), ethynylbenzene (**4a**) (0.058 g, 0.56 mmol), DBU (0.086 g, 0.56 mmol), Cul (0.003 g, 0.014 mmol) and Pd-EncatTM TPP30 (0.025 g, 0.009 mmol), derivative **1a** (0.083 g, 75%) was obtained as an orange solid. M. p.: 100–102 °C. ¹H-NMR (CDCl₃, ppm) δ : 8.49 (d, J = 7.8 Hz, 2H, *o*-NPh), 7.67–7.69 (m, 4H, *o*-Ph), 7.60 (s, 2H, H-5 and -6), 7.56 (t, J = 7.8 Hz, 2H, *m*-NPh), 7.47 (t, J = 7.8 Hz, 1H, *p*-NPh), 7.36–7.42 (m, 6H, *m,p*-Ph). ¹³C-NMR (CDCl₃, ppm) δ : 145.1, 140.1, 131.9, 130.6, 129.3, 128.8, 128.4, 128.3, 122.9, 121.0, 114.2, 96.7, 85.3. HRMS calcd for C₂₈H₁₇N₃ M⁺ 395.465, found 395.903.

2-Phenyl-4,7-bis((3,4,5-trimethoxyphenyl)ethynyl)-2H-

benzo[d][1,2,3]triazole (1c): From 4,7-dibromo-2-phenyl-2H-benzo[d][1,2,3]triazole (**3a**) (0.100 g, 0.28 mmol), 5-ethynyl-1,2,3-trimethoxybenzene (**4b**) (0.109 g, 0.56 mmol), DBU (0.086 g, 0.56 mmol), Cul (0.003 g, 0.014 mmol) and Pd-EncatTM TPP30 (0.025 g, 0.009 mmol), derivative **1c** (0.133 g, 82%) was obtained as a yellow solid. M. p.: 85–86 °C. ¹H-NMR (CDCl₃, ppm) δ : 8.49 (d, J = 7.6 Hz, 2H, *o*-NPh), 7.62 (s, 2H, H-5 and -6), 7.59 (t, J = 7.6 Hz, 2H, *m*-NPh), 7.50 (t, J = 7.6 Hz, 1H, *p*-NPh), 6.93 (s, 4H, *o*-Ph), 3.93 (s, 12H, *m*-OCH₃), 3.91 (s, 6H, *p*-OCH₃). ¹³C-NMR (CDCl₃, ppm) δ : 153.0, 144.9, 140.0, 139.3, 130.6, 129.4, 129.3, 120.9, 117.7, 114.0, 109.1, 96.7, 84.3, 60.9, 56.2. HRMS calcd for C₃₄H₂₉N₃O₆ M⁺ 575.621 found 575.176.

2-(4'-Bromo-[1,1'-biphenyl]-4-yl)-4,7-bis(phenylethynyl)-2H-

benzo[d][1,2,3]triazole (1e): From 4,7-dibromo-2-(4'-bromo-[1,1'-biphenyl]-4-yl)-2H-benzo[d][1,2,3]triazole (**3b**) (0.100 g, 0.2 mmol), ethynylbenzene (**4a**) (0.041 g, 0.40 mmol), DBU (0.060 g, 0.39 mmol), Cul (0.002 g, 0.010 mmol) and Pd-EncatTM TPP30 (0.020 g, 0.007 mmol), derivative **1e** (0.083 g, 88%) was obtained as a brown solid. M. p.: 194–196 °C. ¹H-NMR (CDCl₃, ppm) δ : 8.57 (d, J = 8.7 Hz, 2H, *o*-NPh), 7.75 (d, J = 8.7 Hz, 2H, *m*-NPh), 7.69–7.71 (m, 4H, *o*-Ph), 7.62 (s, 2H, H-5 and -6), 7.61 (d, J = 8.3 Hz, 2H, *m*-BrPh), 7.54 (d, J = 8.3 Hz, 2H, *o*-BrPh), 7.40–7.42 (m, 6H, *m,p*-Ph). ¹³C-NMR (CDCl₃, ppm) δ : 145.1, 140.9, 139.4, 138.7, 132.0, 131.9, 130.7, 128.8, 128.6, 128.4, 127.7, 122.9, 122.2, 121.4, 114.1, 96.7, 85.3. HRMS calcd for C₃₄H₂₀BrN₃ M⁺ 550.459, found 550.984.

2-(4'-Bromo-[1,1'-biphenyl]-4-yl)-4,7-bis((3,4,5-trimethoxyphenyl)ethynyl)-2H-benzo[d][1,2,3]triazole

(1f): From 4,7-dibromo-2-(4'-bromo-[1,1'-biphenyl]-4-yl)-2H-benzo[d][1,2,3]triazole (**3c**) (0.100 g, 0.2 mmol), 5-ethynyl-1,2,3-trimethoxybenzene (**4b**) (0.058 g, 0.40 mmol), DBU (0.060 g, 0.39 mmol), Cul (0.002 g, 0.010 mmol) and Pd-EncatTM TPP30 (0.020 g, 0.007 mmol), derivative **1f** (0.122 g, 83%) was obtained as a yellow solid. M. p.: 128–130 °C. ¹H-NMR (CDCl₃, ppm) δ : 8.56 (d, J = 7.8 Hz, 2H, *o*-NPh), 7.75 (d, J = 7.8 Hz, 2H, *m*-NPh), 7.63 (s, 2H, H-5 and -6), 7.61 (d, J = 7.5 Hz, 2H, *m*-BrPh), 7.53 (d, J = 7.5 Hz, 2H, *o*-BrPh), 6.93 (s, 4H, *o*-Ph), 3.93 (s, 12H, *m*-OCH₃), 3.91 (s, 6H, *p*-OCH₃). ¹³C-NMR (CDCl₃, ppm) δ : 153.1, 145.1, 141.0, 139.4, 139.3, 138.6, 132.1, 130.8, 128.6, 127.8, 122.3, 121.5, 117.7, 113.9, 109.2, 96.9, 84.3,

ARTICLE

Journal Name

61.0, 56.2. HRMS calcd for $C_{40}H_{32}BrN_3O_6$ M^+ 730.615, found 729.147.

4,7-Bis((3,4,5-trimethoxyphenyl)ethynyl)-2-(4'-((3,4,5-trimethoxyphenyl)ethynyl)-[1,1'-biphenyl]-4-yl)-2H-benzo[d][1,2,3]triazole (1g): From 4,7-dibromo-2-(4'-bromo-[1,1'-biphenyl]-4-yl)-2H-benzo[d][1,2,3]triazole (**3c**) (0.100 g, 0.2 mmol), 5-ethynyl-1,2,3-trimethoxybenzene (**4b**) (0.115 g, 0.69 mmol), DBU (0.060 g, 0.39 mmol), CuI (0.002 g, 0.010 mmol) and Pd-EncatTM TPP30 (0.020 g, 0.007 mmol), derivative **1g** (0.053 g, 38%) was obtained as a pale yellow solid. M. p.: 145–146 °C. ¹H-NMR (CDCl₃, ppm) δ: 8.58 (d, *J* = 8.7 Hz, 2H, *o*-NPh), 7.82 (d, *J* = 8.7 Hz, 2H, *m*-NPh), 7.64–7.69 (m, 4H, *H*_{arom}), 7.63 (s, 2H, H-5 and -6), 6.93 (s, 4H, *o*-Ph), 6.81 (s, 2H, *o*-Ph), 3.93 (s, 12H, OCH₃), 3.91 (s, 6H, OCH₃), 3.90 (s, 6H, OCH₃), 3.89 (s, 3H, OCH₃). ¹³C-NMR (CDCl₃, ppm) δ: 153.2, 153.1, 145.2, 141.4, 139.5, 139.4, 139.3, 139.0, 132.1, 130.9, 127.9, 127.0, 122.9, 121.5, 118.1, 117.8, 114.0, 109.2, 108.9, 96.9, 90.7, 88.2, 84.4, 61.1, 61.0, 56.3, 56.2. HRMS calcd for $C_{51}H_{43}N_3O_9$ M^+ 841.917, found 841.299.

Acknowledgements

Financial support from the MINECO of Spain (projects CTQ2012-35692 and CTQ2014-52331-R), Junta de Comunidades de Castilla-La Mancha (FEDER funded project PEII-2014-002-A), and DFG (SFG-TRR 61, project C07) is gratefully acknowledged. I. Torres and R. Martín are indebted to MEC for a FPU studentship. M. V. G. thanks the MINECO of Spain for funding her contract through the Ramón y Cajal program and Parque Científico y Tecnológico de Castilla-La Mancha. Moreover, the technical support from High Performance Computing Service of University of Castilla-La Mancha is gratefully acknowledged.

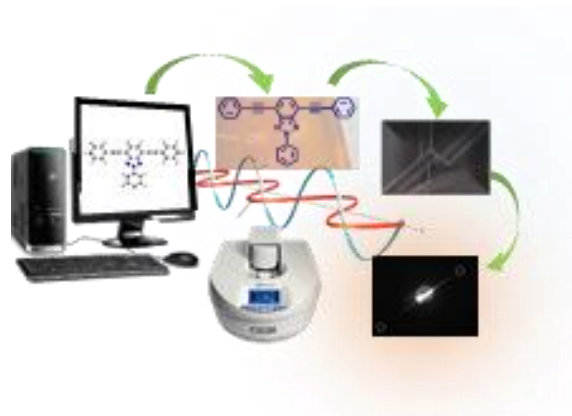
Notes and references

- (a) H. Klauk, *Organic Electronics, Manufacturing and Applications*, (Ed. Wiley-VCH) Weinheim, 2006; (b) H. Klauk, *Organic Electronics II: More Materials and Applications*, (Ed. Wiley-VCH), Weinheim, 2012; (c) A. Facchetti, *Mater. Today*, 2007, **10**, 28–37.
- (a) L. M. Tong, R. R. Gattass, J. B. Ashcom, S. L. He, J. Y. Lou, M. Y. Shen, I. Maxwell and E. Mazur, *Nature*, 2003, **426**, 816–819; (b) J. Y. Zheng, Y. L. Yang, X. P. Wang, Y. S. Zhao, J. X. Huang and J. N. Yao, *J. Am. Chem. Soc.*, 2012, **134**, 2880–2883; (c) X. Xinggui, J. Yao, G. Zhang, Y. Yan, C. Zhang, Q. Peng, Q. Liao, Y. Wu, Z. Xu, Y. Zhao, H. Fu and D. Zhang, *Adv. Funct. Mater.*, 2012, **22**, 4862–4872; (d) Q. Kong, Q. Liao, Z. Xu, X. Wang, J. Yao and H. Fu, *J. Am. Chem. Soc.*, 2014, **136**, 2382–2388; (e) Q. Li, Y. Jia, L. Dai, Y. Yang and J. Li, *ACS Nano*, 2015, **9**, 2689–2695.
- (a) V. Bulovic, V. G. Kozlov, V. B. Khalfin and S. R. Forrest, *Science*, 1998, **279**, 553–555; (b) X. F. Duan, Y. Huang, R. Agarwal and C. M. Lieber, *Nature*, 2003, **421**, 241–245; (c) Y. S. Zhao, A. D. Peng, H. B. Fu, Y. Ma and J. N. Yao, *Adv. Mater.*, 2008, **20**, 1661–1665.
- (a) T. M. Figueira-Duarte and K. Müller, *Chem. Rev.*, 2011, **111**, 7260–7314; (b) W. Z. Yuan, P. Lu, S. M. Chen, J. W. Y. Lam, Z. M. Wang, Y. Liu, H. S. Kwok, Y. G. Ma and B. Z. Yang, *Adv. Mater.*, 2010, **22**, 2159–2163; (c) M. L. Tang and Z. N. Bao, *Chem. Mater.*, 2011, **23**, 446–455.
- C. K. Kao, *Ericsson. Rev.*, 1979, **56**, 92–94.
- N. Chandrasekar and R. Chandrasekar, *Angew. Chem. Int. Ed.*, 2012, **51**, 3556–3561.
- A. Díaz-Ortiz, P. Prieto, J. R. Carrillo, I. Torres and R. Martín, *Curr. Org. Chem.*, 2015, **19**, 568–584.
- (a) T. Yasuda, K. Namekawa, T. Iijima and T. Yamamoto, *Polymer*, 2007, **48**, 4375–4384; (b) L.-R. Tsai and Y. Chen, *Macromolecules*, 2007, **40**, 2984–2992; (c) G. Aromí, L. A. Barrios, O. Roubeau and P. Gamez, *Coord. Chem. Rev.*, 2011, **255**, 485–546; (d) R. R. Kayumova, S. S. Ostakhov, A. V. Mamykin, R. R. Muslukhov, G. F. Iskhakova, S. P. Ivanov, S. A. Meshcheryakova, E. E. Klen, F. A. Khaliullin and V. P. Kazakov, *Russ. J. Gen. Chem.*, 2011, **81**, 1203–1210.
- D. Cáceres, C. Cebrián, A. R. Rodríguez, J. R. Carrillo, A. Díaz-Ortiz, P. Prieto, F. Aparicio, F. García and L. Sánchez, *Chem. Commun.*, 2013, **49**, 621–623.
- M. J. Pastor, I. Torres, C. Cebrián, J. R. Carrillo, A. Díaz-Ortiz, E. Matesanz, J. Buendía, F. García, J. Barberá, P. Prieto and L. Sánchez, *Chem.–Eur. J.*, 2015, **21**, 1795–1802.
- (a) W. Koch and M. C. Holthausen, *A Chemist's Guide to Density Functional Theory*, (Ed. Wiley-VCH Verlag GmbH) Weinheim, Germany, 2001; (b) C. J. Cramer, *Essentials of Computational Chemistry: Theories and Models*, 2nd ed. (Ed. John Wiley & Sons) Chichester, 2005; (c) S. M. Bachrach, *Computational Organic Chemistry*, 2nd ed., (Ed. John Wiley & Sons) Weinheim, Germany, 2014.
- (a) A. Klamt and G. J. Schürmann, *J. Chem. Soc., Perkin Trans. 2*, 1993, 799–805; (b) J. Andzelm, C. Kölmel and A. Klamt, *J. Chem. Phys.*, 1995, **103**, 9312–9320; (c) V. Barone and M. J. Cossi, *Phys. Chem. A*, 1998, **102**, 1995–2001; (d) M. Cossi, N. Rega, G. Scalmani and V. J. Barone, *Comput. Chem.*, 2003, **24**, 669–681.
- C. Adamo and D. Jacquemin, *Chem. Soc. Rev.*, 2013, **42**, 845–856.
- Y. Zhao and D. G. Truhlar, *Theor. Chem. Acc.*, 2008, **120**, 2785–2795.
- (a) R. Li., J. Zheng and D. G. Truhlar, *Theor. Chem. Acc.*, 2008, **120**, 215–241; (b) N. Martínez de Baroja, S. Franco, J. Garín, J. Orduna, B. Villacampa, P. Borja and R. Alicante, *RSC Adv.*, 2013, **3**, 2953–2962.
- S. Grimme, *J. Comp. Chem. A*, 2006, **27**, 1787–1799.
- (a) R. Ditchfield, W. J. Hehre and J. A. Pople, *J. Chem. Phys.*, 1971, **54**, 724–728; (b) W. J. Hehre, R. Ditchfield and J. A. Pople, *J. Chem. Phys.*, 1972, **56**, 2257–2261.
- R. Luschtinetz and G. Seifert, *Comp. Theor. Chem.*, 2013, **1023**, 65–73.
- H. Wettach, F. Pasker and S. Höger, *Macromolecules*, 2008, **41**, 9513–9515.
- W. S. Price, *Concepts Magn. Reson.*, 1998, **10**, 197–237.
- J. A. Castro-Osma, C. Alonso-Moreno, M. V. Gomez, I. Marquez-Segovia, A. Otero, A. Lara-Sanchez, J. Fernandez-Baeza, L. F. Sanchez-Barba and A. M. Rodriguez, *Dalton Trans.*, 2013, **42**, 14240–14252.
- Gaussian 09, Revision A.1, M. J. Frisch, G. W. Trucks, H. B. Schlegel, G. E. Scuseria, M. A. Robb, J. R. Cheeseman, G. Scalmani, V. Barone, B. Mennucci, G. A. Petersson, H. Nakatsuji, M. Caricato, X. Li, X. H. P. Hratchian, A. F. Izmaylov, J. Bloino, G. Zheng, J. L. Sonnenberg, M. Hada, M. Ehara, K. Toyota, R. Fukuda, J. Hasegawa, M. Ishida, T. Nakajima, Y. Honda, O. Kitao, H. Nakai, T. Vreven, Jr. J. A. Montgomery, J. E. Peralta, F. Ogliaro, M. Bearpark, J. J. Heyd, E. Brothers, K. N. Kudin, V. N. Staroverov, R. Kobayashi, J. Normand, K. Raghavachari, A. Rendell, A. J. C. Burant, S. S. Iyengar, S. J. Tomasi, M. Cossi, N. Rega, N. J. Millam, M. Klene, J. E. Knox, J. B. Cross, V. Bakken, C. Adamo, J. Jaramillo, R. Gomperts, R. E. Stratmann, O. Yazyev, O. A. J. Austin, R. Cammi, C. Pomelli, J. W. Ochterski, R. L. Martin,

Journal Name

ARTICLE

- K. Morokuma, V. G. Zakrzewski, G. A. Voth, P. Salvador, J. J. Dannenberg, S. Dapprich, A. D. Daniels, O. Farkas, J. B. Foresman, J. V. Ortiz, J. Cioslowski and D. J. Fox, Gaussian, Inc., Wallingford CT, 2009.
- 23 R. G. Parr and W. Yang, In Density-Functional Theory of Atoms and Molecules, (Oxford University Press) New York, 1994.



View Article Online
DOI: 10.1039/C6RA02473D

Self-assembly of T-shape 2H-benzo[d][1,2,3]-triazoles.

Optical waveguide and photophysical properties.

I. Torres,^a J. R. Carrillo,^a A. Díaz-Ortiz,^a R. Martín,^a M. V. Gómez,^a

L. Stegemann,^b C. A. Strassert,^b J. Orduna,^c J. Buendía,^d

E. E. Greciano,^d J. S. Valera,^d E. Matesanz,^e L. Sánchez*^d and P. Prieto*^a